Sensory Sensitivity to the Form of β-Ga$_2$O$_3$ Nanoparticles

R. Balabai and M. Naumenko

Kryvyi Rih State Pedagogical University,
54, Gagarin Ave.,
UA-50086 Kryvyi Rih, Ukraine

The electronic characteristics of pure β-Ga$_2$O$_3$ nanoparticles with the same number of atoms but of different shapes (spherical or prism-like forms) and with the addition of CO, NH$_3$, O$_3$ molecules near the Ga atom or the O atom are investigated by means of the methods of the theories of electron density functional and pseudopotential from the first principles with application of the own program code. As found, the nanoparticles of both forms can serve as effective resistive detectors of CO and NH$_3$ molecules. A brighter reaction to the CO molecule is recorded in a spherical particle, and a brighter reaction to the NH$_3$ molecule is recorded in a prism-like particle. In this case, the sensitive place of the nanoparticles is located near the Ga atoms, whereas only the spherical nanoparticles effectively respond to O$_3$ molecules by increasing their conducting properties. In this case, the sensitive place of the nanoparticles is located near the O atoms.

З використанням методів теорій функціоналу електронної густини та псевдопотенціялу із перших принципів в рамках власного програмного коду досліджено електронні характеристики наночастинок β-Ga$_2$O$_3$, що містили однакову кількість атомів, але були різних форм (сферичної та призмоподібної), в оточенні газових молекул CO, NH$_3$, O$_3$, що локалізувалися поблизу атомів Ga або O, чи то без молекул. Було встановлено, що наночастинки обох форм можуть служити ефективними резистивними детекторами молекул CO й NH$_3$. Більш яскраву реакцію на молекули CO було зафіксовано у сферичної частинки, а щодо молекул NH$_3$ — у призмоподібної частинки. Воднораз активна ділянка наночастинок як детекторів локалізувалася біля атомів Ga. На молекули O$_3$ ефективно реаґували тільки сферичні наночастинки, збільшуючи свою провідність. У цьому випадку активна ділянка наночастинок локалізувалася біля атомів O.

Key words: β-Ga$_2$O$_3$ nanoparticles of spherical or prism-like forms, molecules of gases, resistive detectors, electronic characteristics, *ab initio* calculations.

1. INTRODUCTION

The sensitivity of the β-Ga$_2$O$_3$ semiconductor to a variety of gases arises because of surface reactions with molecules of gases, which lead to a chemoresistive change in its conductivity. Recent studies have shown that morphology of nanomaterials has a significant effect on the gas sensitivity of nanostructures [1]. Therefore, sensors that are based on flat films have numerous disadvantages, including a limited surface, where there is an interaction between gas molecules and the material, which leads to limited characteristics of the sensors. 1D-semiconductor materials have a high surface-to-volume ratio, which could provide significant sensor feedback. Regarding the synthesis of the 1D Ga$_2$O$_3$ nanostructures, they can be obtained by various methods, including physical evaporation, arc discharge, laser ablation, chemical vapour deposition, grinding, and thermal decomposition of GaN powders.

Information on the use of semiconductor gas sensors of various gas controls on the environment shows that the most important today is the definition of toxic gases (CO, NH$_3$, O$_3$). Adeel Afzal [2] noted that over the past 30 years, the development of miniaturized electronic gas sensors that can detect very low concentrations (≤ 100/ppm to ≥ 0.1/ppb level) of the toxic gases as well as oxygen in the indoor/outdoor environment and automotive/industrial processes have remained the focus of research [3−17]. Semiconductor metal oxides exhibit rapid changes in their electrical properties in response to small changes in the surrounding gas atmosphere.

One of the most developed sensory devices for monitoring harmful greenhouse gases (GHGs) is carbon monoxide (CO). Very important is monitored, which require the development of specific sensor devices, which must meet the following criteria: reliable, responsive, highly sensitive, miniaturized, low cost, and capable to operate on a large range of temperature, from ambient temperature (smart objects) to high temperatures (up to 600°C for industrial combustion processes) [1].

Ozone (O$_3$) is toxic to living organisms, when it is in very low concentrations, causing irritation of respiratory system, headache and burning eyes. Continuing exposure to O$_3$ increases the risk of respiratory diseases, and at high concentrations of O$_3$, has lethal effects. OSHA places the PEL at 0.1 ppm, and the NIOSH's REL is

0.1 ppm [18]. Ammonia (NH$_3$) is an irritant gas and its influence increases with its concentration, also is one of the most common chemicals manufactured and supplied to diverse areas around globe with usage for nitrogen-based fertilizers, pharmaceuticals, cleaning products, refrigeration and explosives.

According to Occupational Safety and Health Administration, exposure beyond 25 ppm for 8 h and 35 ppm for 10 min can harm the skin, eyes and lungs due to highly toxic and corrosive properties of NH$_3$ [19].

Monoclinic gallium oxide (Ga$_2$O$_3$) is a perspective wide band gap ($E_g \approx 4.9$ eV) semiconductor material. Pure or doped Ga$_2$O$_3$ has wide applications in transparent conducting electrodes [20], phosphors [21], gas sensors [22–25], *etc*. Ga$_2$O$_3$ thin film-based gas sensors are very promising to detect oxygen at high temperature of 600–1000°C [26, 27]. It can also be used to detect reducing gases such as H$_2$, CO, CH$_4$, *etc*. [28, 29] at high temperature.

One-dimensional (1D) nanomaterials are considered as ideal candidates for gas sensing applications due to their large surface area-to-volume ratio and the size effect [30]. The 1D nanostructures of well-established gas sensing materials such as SnO$_2$ [30, 31], ZnO [32], WO$_3$ [33, 34], and In$_2$O$_3$ [35] have shown higher sensitivity, faster response, and/or enhanced capability to detect low concentration gases compared with the corresponding thin film materials. Furthermore, gas sensors made from 1D nanomaterials showed lower optimal operating temperature, which is favourable for power saving and device integration. The 1D Ga$_2$O$_3$ nanomaterials have been studied widely in recent years [36–38]. However, few works focus on their gas sensing properties. In work of Zhifu Liu *et al.* [39], in order to make gas sensors, the nanowires were collected and dispersed in methanol with the assistance of ultrasonic. Gas sensors were fabricated by dispensing the Ga$_2$O$_3$ nanowire suspension onto oxidized Si substrates with interdigitated Pt electrodes as described in Ref. [40].

In the article [41], authors reported on a simple method to prepare submicrometer-size spherical β-Ga$_2$O$_3$ particles with uniform diameters. The spherical Ga$_2$O$_3$ particles exhibit a broad blue-green light emission and a peculiar red light emission due to the oxygen vacancies and nitrogen doping formed during the high-temperature growth process in ambient air. The luminescence of the particles can be further tuned by post-annealing of the as grown particles in ammonia atmosphere. Tingting Zhang *et al.* [41] believe that the single-crystalline spherical Ga$_2$O$_3$ particles with excellent luminescence properties are suitable for applications in white-LED phosphors and novel optoelectronic devices.

This work is devoted to the theoretical study, using the methods

of electron density functional, *ab initio* pseudopotential and the author's software [42], the sensitivity of β-Ga_2O_3 nanoparticles of spherical or prism-like forms to the adsorption of CO, NH_3, and O_3 molecules.

2. METHODS AND OBJECTS OF RESEARCH

The basic states of the electron−nucleus systems of β-Ga_2O_3 nanoparticles with CO, NH_3, O_3 molecules were detected by means of the self-consistent solution of the Kohn−Sham equations. Electronic variables only were determined with the atomic cores fixed. Following Kohn−Sham [43, 44], electronic density was written down in terms of occupied orthonormal one-particle wave functions. In the solution of these equations, the pseudopotential formalism was used, according to which a solid is considered as a set of valence electrons and the ion cores. We use Bachelet, Hamann and Schlüter *ab initio* pseudopotential. The total crystalline potential is constructed as the sum of ion pseudopotentials, which are not overlapping and associated with ions (nucleus + core electrons), located at the positions, which are periodically repeated for crystals. For non-periodic systems, such as a thin film or a cluster the problem of lack of periodicity is circumvented by use of the supercell method. Namely, the cluster is periodically repeated but the distance between each cluster and its periodic images is so large that their interaction is negligible. The ubiquitous periodicity of the crystal (or artificial) lattice produces a periodic potential and thus imposes the same periodicity on the density (implying Bloch's theorem). The Kohn−Sham potential of a periodic system exhibits the same periodicity as the direct lattice and the Kohn−Sham orbitals can be written in Bloch's form. This heavily suggests using plane waves as the generic basis set in order to expand the periodic part of the orbitals. Since plane waves form a complete and orthonormal set of functions, they can be used to expand orbitals [45, 46].

The artificial superlattice method was used in present calculations. Therefore, in the studied atomic systems, the artificial translational symmetry was introduced by constructing of a super-lattice with a primitive tetragonal cell and the atomic basis, which contains the complete information about the studied system [47]. The cell was translated in three orthogonal directions.

The conditions for performing present calculations were as follows: integration on the Brillouin zone was replaced by a calculation at one point of the Brillouin zone, namely, at the Γ-point. The iterations stop self-consistent provided matches the current iteration of the calculation results and previous with pre-selected accuracy, their number varied depending on the calculated object, but present

results coincided after 3−5 iteration, usually. The number of plane waves in the schedule of the wave function was truncated by trial calculations and evaluation of the physicality of the obtained results (spatial distribution of electron density, the magnitude of the gap in the electronic energy spectrum between the last occupied state and the first unoccupied), from general ideas about simulated nanostructure or in comparison with the results obtained by other authors. Often, the number of plane waves is chosen to be about 20−25 waves per base atom.

This calculation algorithm for electronic properties is easier to perform in Cartesian space (X, Y, Z), while the performance of crystallographic symmetry operations are performed with fractional crystallographic co-ordinates (x, y, z). In orthonormal crystallographic systems (cubic, tetragonal and orthorhombic), the transformation of coordinates is reduced to a simple division of coordinate values into corresponding cell constants. For example, $x = X/a$, and $X = ax$. In the case of a general oblique crystallographic system, the transformation is described by matrix operations [48].

The monoclinic β-Ga$_2$O$_3$ with space group C2/m has two non-equivalent Ga sites: Ga1 is the six-fold-co-ordinated site, while Ga2 is the fourfold. In addition, there are three non-equivalent O sites, which are threefold-coordinated O1 and O3 sites, while O2 is the four-fold. The lattice parameters at room temperature are measured to be $a = 12.23$ Å, $b = 3.04$ Å, $c = 5.80$ Å, and the unique axis β = 103.7° (angle between a and c axes) unit cell. The unit cell contains four formula units, eight Ga atoms and twelve O atoms are evenly distributed into two Ga and three O non-equivalent sites at positions 4i, (0 0 0), (1/2 1/2 0), (x 0 z) [49−51] (Table).

Fractional crystallographic coordinates of atoms are given in Table. We were transformed into Cartesian co-ordinates using the algorithm described in the work [48]. Discussed there transformation

TABLE. Non-equivalent atomic fractional positions of β-Ga$_2$O$_3$ [48].

Atom	x	y	z	Co-ordination
Ga1	0.09050 (2)	0	0.79460 (5)	four-fold
Ga2	0.15866 (2)	1/2	0.31402 (5)	six-fold
O1	0.1645 (2)	0	0.1098 (3)	three-fold
O2	0.1733 (2)	0	0.5632 (4)	four-fold
O3	0.0041 (2)	1/2	0.2566 (3)	three-fold

of the coordinates of atoms from a crystallographic monoclinic system to Cartesian geometry is not distorted crystal particles of two forms: spherical and prism-like. Therefore, the resulting set of atomic Cartesian co-ordinates can be used to calculate the characteristics of the crystal electron subsystem using the present author's computer program.

Since the laboratory coordinate system operating within the author's software package is **rectangular,** and the calculation algorithm provides translational symmetry, an artificial orthorhombic superlattice was first developed. The object of study is to determine the parameters of this superlattice and atomic basis. Present objects of study were nanoparticles of β-Ga_2O_3 of spherical or prism-like forms with adsorption of CO, NH_3, O_3 molecules. Therefore, the size of the primitive cell was elected so that translated particles do not affect one another due to the built-in vacuum cell gap. In Figure 1, primitive cells of artificial superlattices of orthorhombic type are shown, which reproduced the crystallographic space of finite β-Ga_2O_3 particles of monoclinic system with the space group C2/m of different shapes but with the same number of atoms (contains 30 atoms). It was believed that the β-Ga_2O_3 nanoparticles retain a monoclinic character in their structure regardless of their size and form.
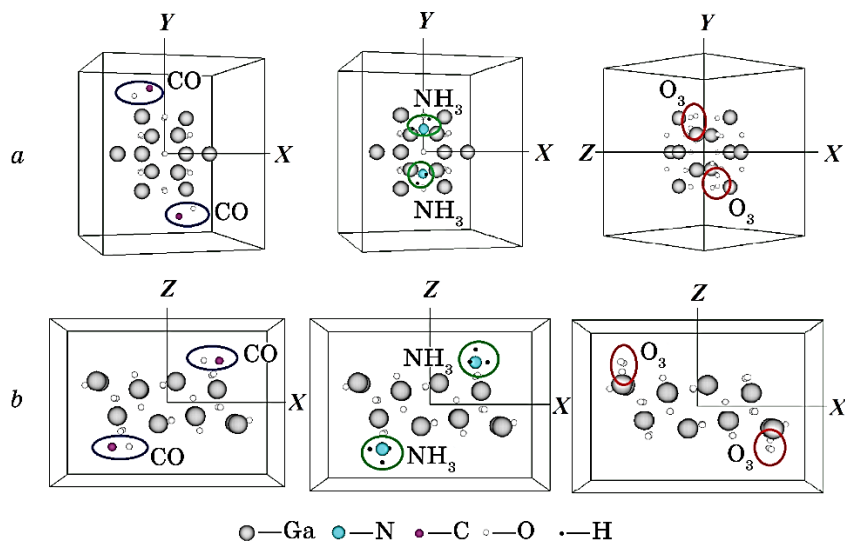
For calculations such objects were developed:

Fig. 1. Primitive cells of an artificial superlattice of the orthorhombic type, which reproduced the crystallographic space of the β-Ga_2O_3 nanoparticle of monoclinic system with pushed CO, NH_3, O_3 molecules (spherical form—top row (*a*), prism-like form—bottom row (*b*)).

— object 1: pure particles of the spherical or prism-like forms with the same number of atoms (30 atoms); the primitive cell of the superlattice with parameters $a = b = c = 24$ Å and $a = 32$ Å, $b = c = 20$ Å, respectively;

— object 2, 5: sphere and prism of Ga$_2$O$_3$ with the addition of carbon monoxide (CO) molecules near gallium and near oxygen, the base consisted of 34 atoms, among them (Ga—12, O—20, C—2); the primitive cell of the superlattice with parameters $a = c = 24$ Å, $b = 28$ Å and $a = 32$ Å, $b = 21$ Å, $c = 23$ Å, respectively;

— object 3, 6: sphere and prism of Ga$_2$O$_3$ with the addition of ammonia (NH$_3$) molecules near gallium and near oxygen, the base consisted of 38 atoms, among them (Ga—12, O—18, N—2, H—6);

— object 4, 7: sphere and prism of Ga$_2$O$_3$ with the addition of ozone (O$_3$) molecule near gallium and near oxygen, the base consisted of 36 atoms, among them (Ga—12, O—24).

The distances between the nearest atoms of molecules and particles were equal to the sums of the radii of the corresponding atoms.

3. RESULTS AND DISCUSSION

The electron density of the studied atomic systems was self-consistent for several periods of iterations, and the atomic base was not optimized. Calculated spatial distributions of valence electron densities and their cross sections within a primitive cell are shown
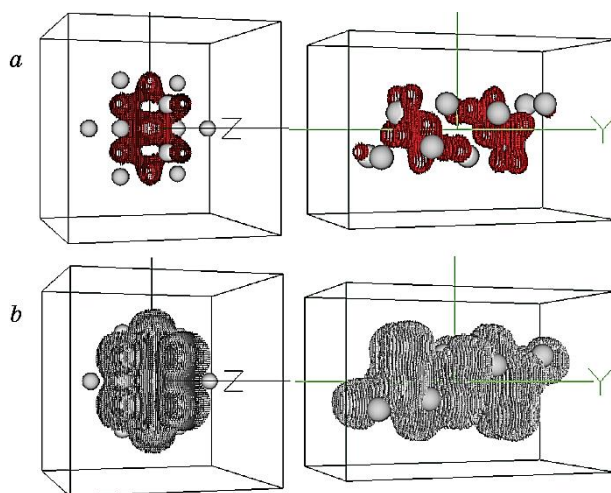

Fig. 2. Spatial density distributions of valence electrons (for the 0.7−0.8 part of the maximum value, top (*a*); for the 0.1−0.2 part of the maximum, down (*b*)) of pure spherical or prism-like forms.
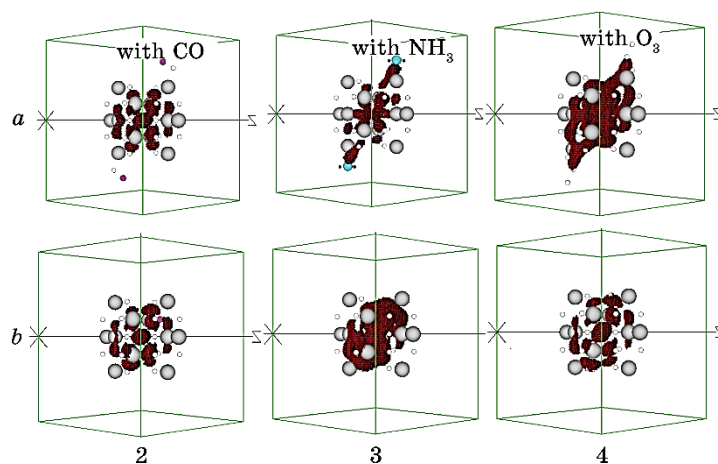
Fig. 3. Spatial distributions of valence electron density within the interval 1.0–0.9 of the maximum value; molecules are located in the vicinity of the gallium atom (*a*) and oxygen atom (*b*) as spherical shape objects 2–4.
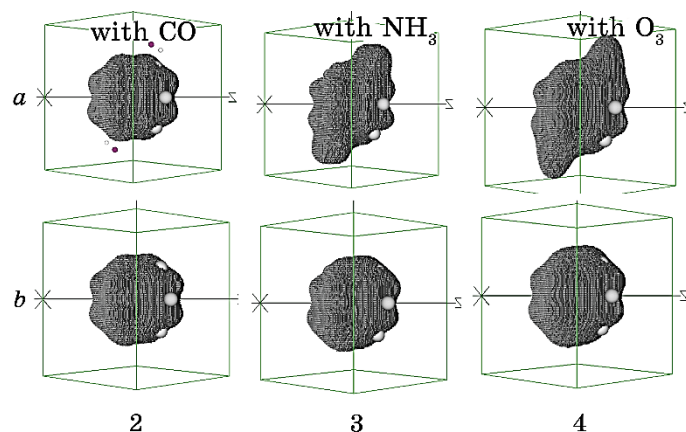

Fig. 4. Spatial distributions of valence electron density within the interval 0.2–0.1 of the maximum value; molecules are located in the vicinity of the gallium atom (*a*) and oxygen atom (*b*) as objects 2–4.

in Figs. 2–7.

Comparing the spatial distributions of the density of valence electrons in pure nanoparticles for the smallest values relative to the maximum value (this electron density is considered to be the one that limits the atomic object), we see that the electron density in spherical particles is more drawn inward than in prismatic particles (Fig. 2).

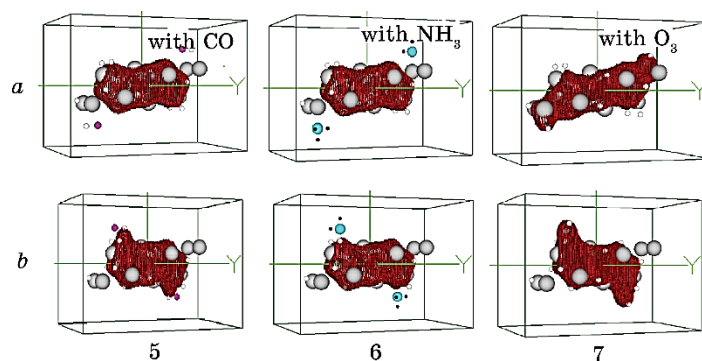The presence of molecules near nanoparticles causes additional

Fig. 5. Spatial distributions of valence electron density within the interval 1.0–0.9 of the maximum value; molecules are located in the vicinity of the gallium atom (*a*) and oxygen atom (*b*) as prism-like forms' objects 5–7.
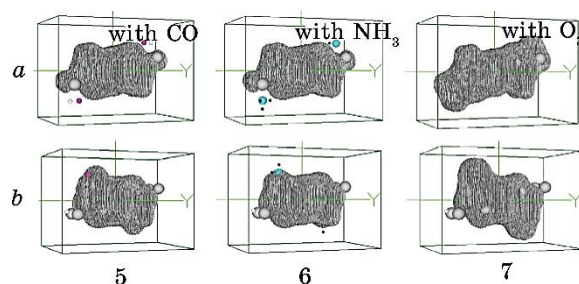

Fig. 6. Spatial distributions of valence electron density within the interval 0.2–0.1 of the maximum value; molecules are located in the vicinity of the gallium atom (*a*) and oxygen atom (*b*) as prism-like shape objects 5–7.

structuring of the spatial distribution of electron density in the middle of the spherical particles (**Fig. 3**).

On the other hand, the presence of molecules near prismatic nanoparticles leads the spatial distribution of the electron density to a more diffuse (uniform) form with the effect of drawing the electron density into the interior of the particles (**Fig. 5**).

It should be noted that, only for the composition 'ozone + + nanoparticle (of any shape)', a combined form of the spatial distribution of valence electrons is formed (**Fig. 4, 6**).

The energy distances between the last main occupied valence electron state and the first unoccupied excited state (band gap) of objects of spherical and prism-like forms with molecules are shown in **Fig. 8**.

It was found that nanoparticles of both forms could serve as effective resistive detectors of CO and NH_3 molecules. At the same
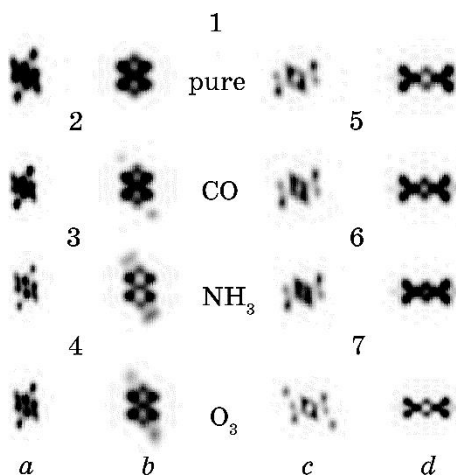
Fig. 7. Cross-sections of spatial distributions of the density of valence electrons within a Ga$_2$O$_3$: (*a*), (*c*)—plane (110) cross-section for objects 1–7, (*b*), (*d*)—plane (100) cross-section for objects 1–7.

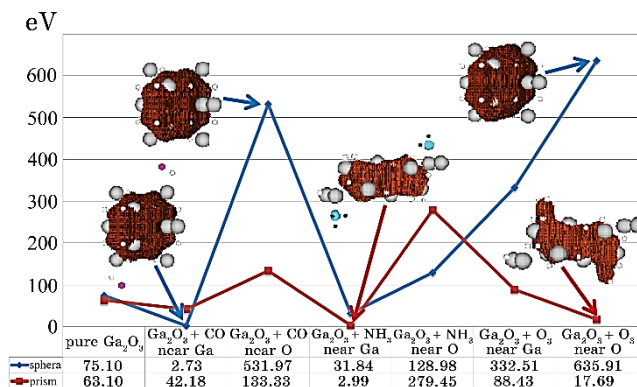|	pure Ga$_2$O$_3$	Ga$_2$O$_3$ + CO near Ga	Ga$_2$O$_3$ + CO near O	Ga$_2$O$_3$ + NH$_3$ near Ga	Ga$_2$O$_3$ + NH$_3$ near O	Ga$_2$O$_3$ + O$_3$ near Ga	Ga$_2$O$_3$ + O$_3$ near O
sphera	75.10	2.73	531.97	31.84	128.98	332.51	635.91
prism	63.10	42.18	133.33	2.99	279.45	88.43	17.69

Fig. 8. Energy distance between the last ground valence electron occupied state and the first unoccupied excited state (band gap) of objects of spherical and prism-like forms with molecules. Inserts contain spatial distribution of valence electron density within the interval of 0.9–0.8 of the maximum value.

time, we considered that the composition 'molecule + particle' was not physically realizable if we recorded very large values of the forbidden energy bands. A decrease in the size of the region of forbidden energies below the value inherent in a crystal ($E_g \approx 4.9$ eV) was considered a constructive reaction.

A brighter reaction to the CO molecule was recorded in a spherical particle, and to the NH$_3$ molecule was recorded in a prism-like

particle. In this case, the sensitive place of the nanoparticles is located near the Ga atoms, whereas only spherical nanoparticles respond effectively to O$_3$ molecules by increasing their conducting properties. In this case, the sensitive place of the nanoparticles is located near the O atoms.

4. CONCLUSION

The electronic characteristics of pure β-Ga$_2$O$_3$ nanoparticles of spherical or prism-like forms with the same number of atoms and with the addition of CO, NH$_3$, O$_3$ molecules near the Ga atom or the O atom were investigated by methods of the theory of electron density functional and pseudopotential from the first principles on the original program code.

The β-Ga$_2$O$_3$ nanoparticles of both forms can serve as effective resistive detectors of CO and NH$_3$ molecules. A brighter reaction to the CO molecule was recorded in a spherical particle, and to the NH$_3$ molecule was recorded in a prism-like particle. In this case, the sensitive place of the nanoparticles is located near the Ga atoms, whereas only spherical nanoparticles effectively respond to O$_3$ molecules by increasing their conducting properties. In this case, the sensitive place of the nanoparticles is located near the O atoms.

REFERENCES

1.   Q. Bui, L. Largeau, N. Jegenyes, O. Mauguin, L. Travers, X. Lafosse, C. Dupuis, J.-C. Harmand, M. Tchernycheva, and N. Gogneau, *Appl. Sci.*, **9**: 3528 (2019); https://doi.org/10.20944/preprints201907.0049.v1

2.   A. Afzal, *J. of Materiomics*, **5**: 542 (2019); https://doi.org/10.1016/j.jmat.2019.08.003

3.   T. Waitz, T. Wagner, C.-D. Kohl, and M. Tiemann, *Stud. Surf. Sci. Catal.*, **174**: 401 (2008); https://doi.org/10.1016/S0167-2991(08)80227-3

4.   C. Wang, L. Yin, L. Zhang, D. Xiang, and R. Gao, *Sensors*, **10**: 2088 (2010); https://doi.org/ 10.3390/s100302088

5.   G. F. Fine, L. M. Cavanagh, A. Afonja, and R. Binions, *Sensors*, **10**: 5469 (2010); https://doi.org/10.3390/s100605469

6.   A. Afzal, N. Cioffi, L. Sabbatini, and L. Torsi, *Sens. Actuators B: Chemical*, **171−172**: 25 (2012); https://doi.org/10.1016/j.snb.2012.05.026

7.   *Gas sensing Fundamentals* (Eds. C.-D. Kohl and T. Wagner) (Berlin−Heidelberg: Springer-Verlag: 2014).

8.   A. Mirzaei and G. Neri, *Sens Actuators B: Chemical*, **237**: 749 (2016); https://doi.org/10.1016/j.snb.2016.06.114

9.   A. Mirzaei, S. G. Leonardi, and G. Neri, *Ceram. Int.*, **42**: 15119 (2016); https://doi.org/10.1016/j.ceramint.2016.06.145

10.   P. T. Moseley, *Meas. Sci Technol.*, **28**: 082001 (2017); https://doi.org/10.1088/1361-6501/aa7443

11.   G. Korotcenkov and B. K. Cho, *Sens. Actuators B: Chemical*, **244**: 182
        (2017); https://doi.org/10.1016/j.snb.2016.12.117
12.   J. Zhang, Z. Qin, D. Zeng, and C. Xie, *Phys. Chem. Chem. Phys.*, **19**: 6313
        (2017); https://doi.org/10.1039/C6CP07799D
13.   X. Gao, and T. Zhang, *Sens. Actuators B: Chemical*, **277**: 604 (2018);
        https://doi.org/10.1016/j.snb.2018.08.129
14.   E. Llobet, E. Navarrete, F. E. Annanouch, M. Alvarado, E. González,
        J. L. Ramírez, A. Romero, X. Vilanova, M. Domínguez-Pumar, S. Vallejos,
        and I. Grácia, *2018 IEEE Sens.*, **1**: 8589734 (2018);
        https://doi.org/10.1109/ICSENS
15.   A. Dey, *Mater. Sci Eng. B*, **229**: 206 (2018);
        https://doi.org/10.1016/j.mseb.2017.12.036
16.   A. Oprea, D. Degler, N. Barsan, A. Hemeryck, and J. Rebholz, *Gas Sensors
        Based on Conducting Metal Oxides: Basic Understanding, Technology and
        Applications* (Eds. N. Barsan and K. Schierbaum) (Elsevier: 2019), Ch. 3, p.
        61−165:; https://doi.org/10.1016/B978-0-12-811224-3.00003-2
17.   Z. Li, H. Li, Z. Wu, M. Wang, J. Luo, H. Torun, P. Hu, C. Yang,
        M. Grundmann, X. Liud, and Y. Fu, *Mater. Horiz.*, **6**: 470 (2019);
        https://doi.org/10.1039/C8MH01365A
18.   M. Panayotova, V. Panayotov, and T. Oliinyk, *EDP Sciences*, **166**: 01008
        (2020); https://doi.org/10.1051/e3sconf/202016601008
19.   D. Kwak, Y. Lei, and R. Maric, *Talanta*, **204**: 713 (2019);
        https://doi.org/10.1016/j.talanta.2019.06.034
20.   H. Ohta, K. Nomura, H. Hiramatsu, K. Ueda, T. Kamiya, M. Hirano, and
        H. Hosono, *Solid-State Electron.*, **47**: 2261 (2003);
        https://doi.org/10.1016/S0038-1101(03)00208-9
21.   H. B. Xie, L. M. Chen, Y. N. Liu, and K. L. Huang, *Solid State Commun.*,
        141: 12 (2007); https://doi.org/10.1016/j.ssc.2006.09.046
22.   M. Fleischer and H. Meixner, *Sens. Actuators B: Chemical*, **52**: 179 (1998);
        https://doi.org/10.1016/S0925-4005(98)00271-8
23.   J. Frank, M. Fleischer, H. Meixner, and A. Feltz, *Sens. Actuators B: Chemi-
        cal*, **49**, Iss. 1−2: 110 (1998); https://doi.org/10.1016/S0925-
        4005(98)00094-X
24.   C. Babana, Y. Toyodac, and M. Ogita, *Thin Solid Films*, **484**: 369 (2005);
        https://doi.org/10.1016/j.tsf.2005.03.001
25.   A. Trinchi, W. Wlodarski, and Y. Li, *Sens. Actuators B: Chemical*, **100**: 94
        (2004); https://doi.org/10.1016/j.snb.2003.12.02
26.   T. Schwebel, M. Fleischer, and H. Meixner, *Sens. Actuators B: Chemical*, **65**,
        Iss. 1−3: 176 (2000); https://doi.org/10.1016/S0925-4005(99)00326-3
27.   M. Ogita, K. Higo, Y. Nakanishi, and Y. Hatanaka, *Appl. Surf. Sci.*, **175−
        176**: 721 (2001); https://doi.org/10.1016/S0169-4332(01)00080-0
28.   M. Fleischer, J. Giber, and H. Meixner, *Appl. Phys. A*, **54**: 560 (1992);
        https://doi.org/10.1007/BF00324340
29.   T. Schwebel, M. Fleischer, H. Meixner, and C. D. Kohl, *Sens. Actuators B:
        Chemical*, **49**, Iss. 1−2: 46 (1998); https://doi.org/10.1016/S0925-
        4005(97)00334-1
30.   A. Kolmakov, Y. Zhang, G. Cheng, and M. Moskovits, *Adv. Mater.*, **15**: 997
        (2003); https://doi.org/10.1002/adma.200304889
31.   E. Comini, G. Faglia, G. Sberveglieri, Z. W. Pan, and Z. L. Wang, *Appl.*

Phys. Lett., **81**: 1869 (2002); https://doi.org/10.1063/1.1504867

32.   Q. Wan, Q. H. Li, Y. J. Chen, T. H. Wang, X. L. He, J. P. Li, and
      C. L. Lin, *Appl. Phys. Lett.*, **84**: 3654 (2004);
      https://doi.org/10.1063/1.1748852

33.   A. Ponzoni, E. Comini, G. Sberveglieri, J. Zhou, S. Deng, N. Xu, Y. Ding,
      and Z. Wang, *Appl. Phys. Lett.*, **88**: 20 (2006);
      https://doi.org/10.1063/1.2203932

34.   C. S. Rout, A. Govindaraj, and C. N. R. Rao, *J. Mater. Chem.*, **16**: 3936
      (2006); https://doi.org/10.1039/B607012B

35.   D. H. Zhang, Z. Q. Liu, C. Li, T. Tang, X. L. Liu, S. Han, B. Lei, and
      C. W. Zhou, *Nano Lett.*, **4**: 1919 (2004); https://doi.org/10.1021/nl0489283

36.   H. Z. Zhang, Y. C. Kong, Y. Z. Wang, X. Du, Z. G. Bai, J. J. Wang,
      D. P. Yu, Y. Ding, Q. L. Huang, and S. Q. Feng, *Solid State Commun.*, **109**:
      677 (1999); https://doi.org/10.1016/S0038-1098(99)00015-0

37.   X. C. Wu, W. H. Song, W. D. Huang, M. H. Pu, B. Zhao, Y. P. Sun, and
      J. J. Du, *Chem. Phys. Lett.*, **328**: 5 (2000); https://doi.org/10.1016/S0009-
      2614(00)00899-X

38.   P. Feng, X. Y. Xie, Y. G. Liu, Q. Wan, and T. H. Wang, *Appl. Phys. Lett.*,
      89: 1121141 (2006); https://doi.org/10.1063/1.2349278

39.   Z. Liu, T. Yamazaki, Y. Shen, T. Kikuta, N. Nakatani, and Y. Li, *Sens. Ac-
      tuators B: Chemical*, **129**, Iss. 2: 666 (2008);
      https://doi.org/10.1016/j.snb.2007.09.055

40.   Z. F. Liu, T. Yamazaki, Y. B. Shen, T. Kikuta, N. Nakatani, and
      T. Kawabata, *Appl. Phys. Lett.*, **90**: 173119 (2007);
      https://doi.org/10.1063/1.2732818

41.   T. Zhang, J. Lin, X. Zhang, Y. Huang, X. Xu, Y. Xue, J. Zou, and C. Tang,
      J. of Lumin., **140**: 30 (2013); https://doi.org/10.1016/j.jlumin.2013.02.031

42.   R. Balabai and A. Solomenko, *Appl. Nanosci.*, **9**: 1011 (2019);
      https://doi.org/10.1007/s13204-018-0709-9

43.   P. Hohenberg and W. Kohn, *Phys. Rev.*, **136**, Iss. 3B: B864 (1964);
      https://doi.org/10.1103/PhysRev.136.B864

44.   W. Kohn and L. Sham, *Phys. Rev.*, **140**, Iss. 4A: A1133 (1965);
      https://doi.org/10.1103/PhysRev.140.A1133

45.   R. Balabai, D. Kravtsova, P. Merzlykin and Yu. Prihozhaya,
      J. Nanophoton., **12**, No. 3: 036003 (2018); doi:10.1117/1.JNP.12.036003

46.   R. M. Balabai and D. V. Zalevskyi, *Phys. and Chem. of Solid State*, **20**,
      No. 3: 247 (2019); doi:10.15330/pcss.20.3.247-256

47.   R. M. Balabai, A. V. Zdeshchyts, and D. V. Zalevskyi, *Sem. Phys., Quant.
      Electr. & Optoelectr.*, **21**, No. 1: 65 (2018);
      https://doi.org/10.15407/spqeo21.01.065

48.   R. M. Balabai and M. V. Naumenko, *Photoelectronics*, **29**: 12 (2020);
      https://doi.org/10.18524/0235-2435.2020.29.225463

49.   J. Ahman, G. Svensson, and J. Albertsson, *Acta Cryst.*, **C52**: 1336 (1996);
      https://doi.org/10.1107/S0108270195016404

50.   S. Geller, *J. Chem. Phys.*, **33**: 676 (1960);
      https://doi.org/10.1063/1.1731237

51.   S. Kumar and R. Singh, *Phys. Status Solidi RRL*, **7**, Iss. 10: 781 (2013);
      https://doi.org/10.1002/pssr.201307253